Colin R. Smith
Department of Mechanical Engineering,
University of Wisconsin-Madison,
1513 University Avenue,
Madison, WI 53706
e-mail: crsmith25@wisc.edu

Michael F. Vignos
Department of Mechanical Engineering,
University of Wisconsin-Madison,
1513 University Avenue,
Madison, WI 53706
e-mail: mvignos@wisc.edu

Rachel L. Lenhart
Department of Mechanical Engineering,
University of Wisconsin-Madison,
1513 University Avenue,
Madison, WI 53706;
Department of Biomedical Engineering,
University of Wisconsin-Madison,
1513 University Avenue,
Madison, WI 53706
e-mail: rlenhart@wisc.edu

Jarred Kaiser
Department of Mechanical Engineering,
University of Wisconsin-Madison,
1513 University Avenue,
Madison, WI 53706
e-mail: jmkaiser2@wisc.edu

Darryl G. Thelen[1]
Fellow ASME
Department of Mechanical Engineering,
University of Wisconsin-Madison,
1513 University Avenue,
Madison, WI 53706;
Department of Biomedical Engineering,
University of Wisconsin-Madison,
1513 University Avenue,
Madison, WI 53706;
Department of Orthopedics and Rehabilitation,
University of Wisconsin-Madison,
1513 University Avenue,
Madison, WI 53706
e-mail: dgthelen@wisc.edu

The Influence of Component Alignment and Ligament Properties on Tibiofemoral Contact Forces in Total Knee Replacement

The study objective was to investigate the influence of coronal plane alignment and ligament properties on total knee replacement (TKR) contact loads during walking. We created a subject-specific knee model of an 83-year-old male who had an instrumented TKR. The knee model was incorporated into a lower extremity musculoskeletal model and included deformable contact, ligamentous structures, and six degrees-of-freedom (DOF) tibiofemoral and patellofemoral joints. A novel numerical optimization technique was used to simultaneously predict muscle forces, secondary knee kinematics, ligament forces, and joint contact pressures from standard gait analysis data collected on the subject. The nominal knee model predictions of medial, lateral, and total contact forces during gait agreed well with TKR measures, with root-mean-square (rms) errors of 0.23, 0.22, and 0.33 body weight (BW), respectively. Coronal plane component alignment did not affect total knee contact loads, but did alter the medial–lateral load distribution, with 4 deg varus and 4 deg valgus rotations in component alignment inducing +17% and −23% changes in the first peak medial tibiofemoral contact forces, respectively. A Monte Carlo analysis showed that uncertainties in ligament stiffness and reference strains induce ±0.2 BW uncertainty in tibiofemoral force estimates over the gait cycle. Ligament properties had substantial influence on the TKR load distributions, with the medial collateral ligament and iliotibial band (ITB) properties having the largest effects on medial and lateral compartment loading, respectively. The computational framework provides a viable approach for virtually designing TKR components, considering parametric uncertainty and predicting the effects of joint alignment and soft tissue balancing procedures on TKR function during movement. [DOI: 10.1115/1.4032464]

Introduction

Component alignment and soft tissue balance can affect the function and longevity of total knee replacements (TKR). Excessive varus and valgus malalignments are associated with substantially higher rates of failure [1]. Further, clinical studies have linked soft tissue imbalances with instability and long-term failures of the joint [2–12]. Soft tissue balance is highly dependent on ligament tensioning achieved surgically, with changes in component thickness and soft tissue releases employed to adjust ligament tension and balance [13–17]. However, despite the clinical significance, it remains challenging to assess the effects of component alignment and ligament stiffness on the in vivo behavior of TKR during functional movement. Such information is important to elucidate the underlying mechanical causes of joint failure.

Computational musculoskeletal modeling provides a powerful platform to investigate the sensitivity of TKR behavior during locomotor tasks, such as walking. In contrast to cadaveric experiments, computational modeling can be used to comprehensively assess parametric sensitivities of joint mechanics under functional soft tissue and external loads. Thanks in part to the *Grand Challenge Competition to Predict In Vivo Knee Loads* initiated by Fregly and colleagues [18], models used to predict TKR mechanics have seen notable advances in sophistication and veracity in recent years. Entries to the competition have employed various modeling approaches including inverse optimization models [19], finite-element analysis [20], electromyogram-driven simulations [21], and dynamic simulations that couple movement and joint mechanics [22–24]. However, modeling studies often do not systematically consider the influence that parametric uncertainty [25]

[1]Corresponding author.

Manuscript received October 16, 2015; final manuscript received January 6, 2016; published online January 27, 2016. Editor: Beth A. Winkelstein.

can have on predictions of joint contact forces. Such uncertainty analysis is particularly relevant to assessing ligament effects, given that ligament constitutive properties cannot be measured on a subject-specific basis and large variability exists across the population [26–31].

As part of the 2015 "Grand Challenge," the objective of this study was to investigate the influence of joint alignment and uncertain ligament properties on TKR loading during walking. To do this, we created a subject-specific knee model that included deformable contact, ligamentous structures, and 6DOF tibiofemoral and patellofemoral joints. A novel numerical optimization technique was employed to simultaneously predict muscle forces, secondary knee kinematics, ligament forces, and joint contact pressures from experimental gait analysis measures. Model predictions of tibiofemoral contact forces were compared to subject-specific in vivo measurements obtained from an instrumented joint replacement. We also used a Monte Carlo approach to assess the effect of uncertainties in ligament stiffness and reference strains on both ligament forces and tibiofemoral contact force predictions.

Methods

Experimental Data. The subject of this study was an 83-year-old male with an instrumented right TKR (mass = 70 kg and height = 172 cm). The experimental data were provided by the sixth edition of the *Grand Challenge Competition to Predict In Vivo Knee Loads* [32]. Whole body kinematics and ground reaction forces were measured in a standard motion analysis laboratory while the subject executed two modified styles of overground gait: *smooth* and *bouncy*. The verbal instructions for each walking pattern were to use a "reduced (increased) superior–inferior translation of the pelvis during the gait cycle," respectively [18]. Motion capture marker kinematics were collected at 120 Hz and low-pass filtered with a cutoff frequency of 6 Hz, and ground reaction forces were collected at 1000 Hz and low-pass filtered at a cutoff frequency of 50 Hz. Tibial plateau contact loads were measured simultaneously with the other experimental data by an instrumented tibial component. The measured loads were decomposed into medial and lateral components using an empirical regression equation [33].

Knee Model. A three-body knee model was developed using the implanted component geometries and subject-specific bone geometries segmented from computed tomography (CT) images (Fig. 1). The tibiofemoral and patellofemoral joints were both modeled as 6DOF with deformable contact. An elastic patellar tendon (PT) and 11 elastic ligament bundles were included in the model: anteriolateral and posteriomedial posterior cruciate ligament (aPCL and pPCL), superficial and deep medial collateral ligament (sMCL and dMCL), lateral collateral ligament (LCL), popliteofibular ligament (PFL), posteriomedial capsule (pmCAP), posterior capsule (CAP), iliotibial band (ITB) medial patellofemoral ligament (MPFL), and lateral patellofemoral ligament (LPFL). The anterior cruciate ligament was not included in the model because it was resected during the TKR surgery.

Ligaments were modeled as bundles of strands extending between the origin and insertion attachment footprints. Ellipsoidal wrap objects were included for the sMCL, pmCAP, and LPFL bundles to prevent penetration of the ligament path into the bone and component geometries. A generic ligament force–strain relationship was used, which assumed the ligament force to be quadratic at low strains and linear at high strains [34,35]. For each ligament bundle, linear stiffness and reference strain parameters were defined to scale the generic force–strain curve (Table 1). The linear stiffness defined the slope of the force–strain curve and the reference strain defined the strain of the ligament in a reference posture (extended knee). Reference strains were then used to compute the ligament slack lengths. Linear stiffness was estimated from ligament cross-sectional areas measured from an MRI of a subject of similar stature and an assumed elastic modulus of 125 MPa [26]. Reference strains were adapted from the literature [23,36,37]. Ligament attachment footprints on the bone mesh geometries were estimated based on anatomical studies [38–52]. The attachment points of individual strands were evenly distributed by uniformly sampling B-spline surface representations of the attachment footprints [53].

The articular surface geometries of the tibial, femoral, and patellar components were represented as triangulated meshes (10,000; 21,000; and 8000 triangles, respectively). We performed

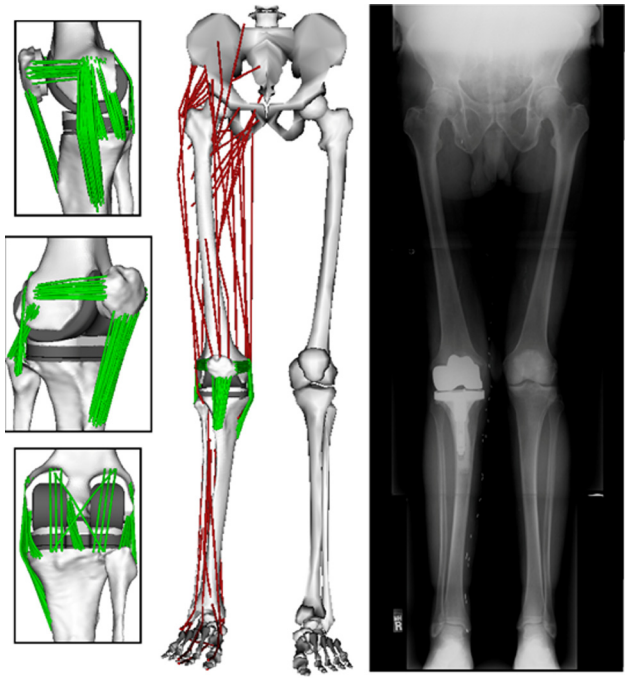

Fig. 1 The knee model used subject-specific bone and TKR component geometry and included an extensible PT and 11 ligament bundles. The knee model was integrated into a generic lower extremity model which included 44 muscle–tendon units acting about the hip, knee, and ankle. The coronal plane TKR component alignment in the nominal model was set to match the limb alignment measured for the subject in a standing radiograph.

Table 1 Ligament and PT properties assumed in the unblinded nominal model. For each ligament, the stiffness was evenly divided between the individual strands included in a bundle. Reference strains reflect the strain assumed for the ligament with the knee in a relaxed extended posture.

	Stiffness (*N*/strain)	Reference strain	
Name	Nominal (95% CI)	Nominal (95% CI)	Number of strands
aPCL	5700 (2280 to 9120)	0.01 (−0.03 to 0.04)	10
pPCL	2400 (960 to 3840)	−0.06 (−0.10 to −0.02)	10
sMCL	2200 (880 to 3520)	0.03 (−0.01 to 0.07)	20
dMCL	2800 (1120 to 4480)	0.03 (−0.01 to 0.07)	10
LCL	1800 (720 to 2880)	0.06 (0.02 to 0.10)	10
PFL	3000 (1200 to 4800)	−0.01 (−0.05 to 0.03)	10
pmCAP	2000 (800 to 3200)	0.05 (0.01 to 0.09)	10
CAP	4000 (1600 to 6400)	0.08 (0.04 to 0.12)	8
ITB	4000 (1600 to 6400)	0.02 (−0.02 to 0.06)	1
PT	14,700 (5880 to 23,520)	0.02 (−0.02 to 0.06)	30
mPFL	1000 (400 to 1600)	−0.05 (−0.09 to −0.01)	15
lPFL	800 (320 to 1280)	0.01 (−0.03 to 0.05)	15

a set of simulations with increasing mesh densities to determine the minimum number of triangles per mesh required to generate converged contact force predictions. Joint contact surface pressures (p) were calculated on each triangle based on the local surface penetration depth according to the elastic foundation model [54]

$$p = \frac{(1-v)E}{(1+v)(1-2v)}\frac{d}{h} \tag{1}$$

where E is the elastic modulus, v is the Poisson's ratio, h is the thickness of the tibial insert, and d is the penetration depth. The femoral component was assumed to be rigid, and the polyethylene tibial insert was assumed to have a uniform thickness of 9 mm and exhibit linearly elastic material properties. The commonly reported value for elastic modulus of polyethylene inserts ($E = 463$ MPa) [55] was reduced by a factor of 10 to improve the numerical stability of contact in the gait simulations. The Poisson's ratio was 0.46 [56]. Contacting regions between the articulating surface meshes were determined using ray-casting techniques in conjunction with hierarchical object orientated bounding boxes [23].

Lower Extremity Musculoskeletal Model. The knee model was integrated into a generic lower extremity musculoskeletal model [57] which consisted of pelvis, thigh, shank, and foot segments. The hip was modeled as a 3DOF ball and socket joint and the ankle as a 1DOF pin joint. The thigh and shank segments were scaled such that the generic tibia and femur geometries matched the subject-specific bones. All the remaining segments were scaled to minimize the differences between anatomical landmarks on the generic model and anatomical marker positions measured with the subject in a static upright posture. The subject-specific femur and tibia were manually aligned to the scaled generic bones. The femoral and tibial components were placed such that the limb alignment in the coronal plane matched the hip–knee–ankle angle measured from a standing radiograph [58] (Fig. 1). The patella was manually positioned relative to the femur such that it matched the CT scans in the reference posture.

The generic model included 44 muscle–tendon units crossing the hip, knee, and ankle joints [57]. Individual muscle forces (F) were assumed to linearly scale with activation level (a), i.e., $F = a \cdot F_0$, where F_0 is the maximum isometric force for the muscle (see Supplemental Information available under "Supplemental Data" tab for this paper on the ASME Digital Collection). The full model was implemented in Software for Interactive Musculoskeletal Modeling (SIMM) [59] with the Dynamics Pipeline (Musculographics, Inc., Santa Rosa, CA) and SD/Fast (Parametric Technology Corp., Needham, MA) used to generate the code describing ligament wrapping and the multibody equations of motion.

Gait Simulations. At each frame of the gait cycles, a global optimization inverse kinematics routine determined pelvis translations, pelvis rotations, hip angles, knee flexion angle, and ankle angle that minimized the sum of squared differences between model marker locations and measured marker locations. During inverse kinematics, the secondary tibiofemoral and all patellofemoral kinematics were constrained to be functions of the knee flexion angle. These functions were determined by simulating passive knee flexion (0–70 deg) using the subject-specific knee model.

An enhanced static optimization (ESO) routine was then used to simultaneously predict the muscle forces, secondary tibiofemoral and patellofemoral kinematics, ligament forces, and joint contact pressures at each frame in the gait cycle (Fig. 2). The optimization problem was formulated to solve for muscle activations and secondary knee kinematics which minimized an objective function (J) while satisfying overall dynamic constraints.

$$J = \sum_{i=1}^{n_{muscles}} V_i a_i^2 + w \sum_{j=1}^{n_{faces}} U_j \tag{2}$$

The objective function minimized the muscle volume (V) weighted sum of squared muscle activations (a) [60] plus the net knee joint contact energy. Contact energy (U) associated with each face of a contact mesh was computed as the integral of its force–deformation relationship (Eq. (1)). The net contact energy was then obtained by summing energy over all faces of the articulating surface meshes. In a sensitivity study, we found inclusion

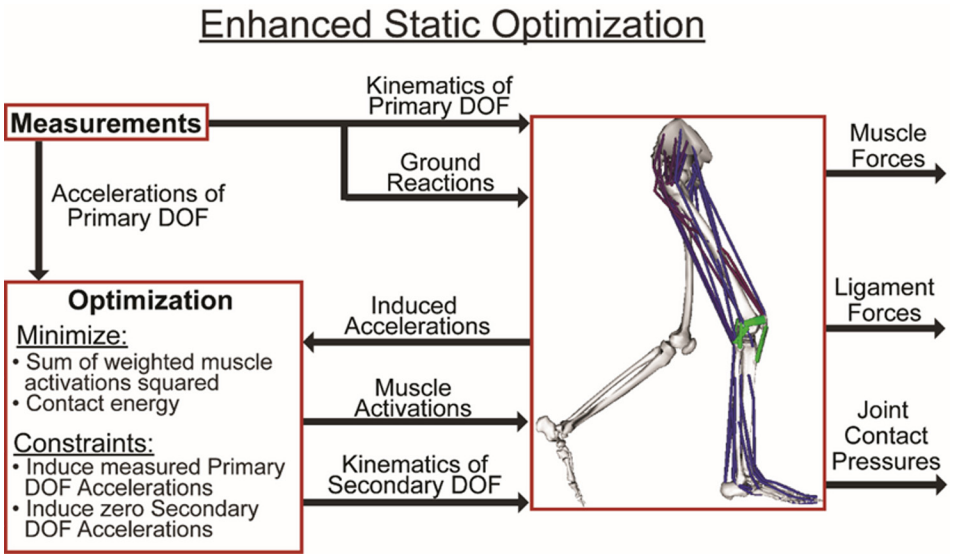

Fig. 2 A numerical optimization approach was used to simultaneously predict patellofemoral kinematics, secondary tibiofemoral kinematics, and muscle forces that, together with the induced ligament forces and contact pressures, generated the measured hip, knee, and ankle accelerations at each time step of a gait cycle. Muscle force distribution was determined by minimizing an objective function that consisted of a sum of volume weighted squared muscle activations and the knee joint contact energy.

of the contact energy term reduced tibiofemoral contact loads, particularly at the second loading peak of stance phase. The regularization scale factor w was held constant for all the simulations at a value for which further increases had relatively small effects on the predicted peak contact loads (see Supplemental Information available under "Supplemental Data" tab for this paper on the ASME Digital Collection). The optimization constraints required that the muscle forces and internal knee loads (contact pressures and ligament forces) produced by the optimized knee kinematics generate the measured hip, knee (flexion), and ankle accelerations while also inducing equilibrium (zero accelerations) in the secondary tibiofemoral and all patellofemoral DOF. Linear viscous damping effects were included on the knee DOF to ensure the generation of smooth frame-to-frame kinematics. Pelvis coordinates were prescribed to reproduce measured values, and measured ground reaction forces and moments were applied directly to the feet. It should be explicitly noted that tibiofemoral and patellofemoral behaviors were not pre-assumed in our simulations, but evolved as a result of the interaction of external, joint contact, ligament, and muscle forces. Thus, each gait simulation provided a prediction of the ligament and contact forces over the entire gait cycle which were then analyzed for the purposes of this study.

Grand Challenge Competition. For the blinded phase of the competition, we incorporated the TKR components into a healthy knee model [61], aligning and orienting the components in way that best fit the natural knee cartilage surfaces. For the unblinded phase, we replaced the bone geometries with the skeletal geometries provided for the subject. We also repositioned the TKR components to both match the articular surfaces based on the subject's CT scans and coronal alignment based on standing radiographs (Fig. 1). We defined the ligament origins, insertions, and wrapping geometries to the subject-specific bone geometries using literature descriptions of normal attachment sites [38–52].

The tibiofemoral medial, lateral, and total contact force predictions of the blinded and unblinded models were quantitatively evaluated against the measured contact forces for the *smooth* and *bouncy* gait styles by computing the bias (average difference in force predictions), precision (standard deviation of the force prediction errors), squared Pearson's correlation coefficient (ρ^2), the coefficient of determination (R^2), and rms errors.

Sensitivity to Coronal Plane Alignment. To assess the influence of coronal plane component alignment on the contact force predictions of the model, we performed a series of simulations with the knee alignment modified 2 deg and 4 deg varus and valgus from the nominal orientation in a standing posture. This was achieved by rotating the femoral component by 1 deg and 2 deg in the coronal plane and counter-rotating the tibial component by an equal amount. Passive forward simulations were performed iteratively with the knee fixed at 0 deg flexion to settle the tibia and patella and establish a new reference posture. For each reference posture, the unaltered reference strain of each ligament was then used to compute ligament slack lengths. *Smooth* and *bouncy* gaits were then resimulated using the inverse kinematics and ESO methods described previously (Fig. 3).

Probabilistic Simulations. The sensitivity of the predicted tibiofemoral contact forces during *smooth* gait to ligament constitutive properties was assessed using the Monte Carlo method. The linear stiffness and reference strains of each ligament bundle were represented by independent Gaussian distributions. The distributions were centered at the nominal model stiffness and reference strain values and the standard deviations were assumed to be 30% of the nominal stiffness and 0.02 strain, respectively [62]. A total of 2000 simulations were performed on a high throughput computing grid using randomly selected values from the constitutive property distributions. The uncertainty in the predicted medial, lateral, and total tibiofemoral contact forces was quantified by calculating the time varying means and standard deviations of all the simulations. The number of simulations was justified by verifying that the mean of the total tibiofemoral contact force at each frame of the gait cycle varied by less than 1% when the final 10% of the Monte Carlo simulations were removed.

We then performed a sensitivity analysis to determine the relative influence of the properties of each ligament on the predicted tibiofemoral contact forces. At both the first and second peaks of tibiofemoral loading during stance, we computed the Pearson's correlation coefficient (R) to quantify the correlation between the stiffness and reference strain of each ligament to the tibiofemoral contact forces (Fig. 4). The Pearson's correlation coefficients range between −1 and 1, with values of 1 indicating a perfect positive correlation, −1 indicating a perfect negative correlation, and 0 indicating no correlation. The absolute values of the Pearson's correlation coefficients were used to determine the relative influence of the stiffness and reference strain of each ligament on the tibiofemoral contact forces.

Results

The blinded model predictions of total tibiofemoral loading mimicked the overall measured temporal patterns, with squared Pearson's correlation coefficients of 0.86 and 0.82 during *smooth* and *bouncy* gaits, respectively (Table 2). However, the blinded predictions were biased toward overpredicting the total contact force magnitude (smooth = 0.28 BW and bouncy = 0.3 BW). Much of the bias arose from overpredicting the loading on the medial compartment throughout the gait cycle, while slightly underpredicting the lateral compartment loading throughout much of stance (Fig. 5). Blinded rms errors were 0.52 BW and 0.29 BW on the medial and lateral compartments, respectively, in the *smooth* gait trial.

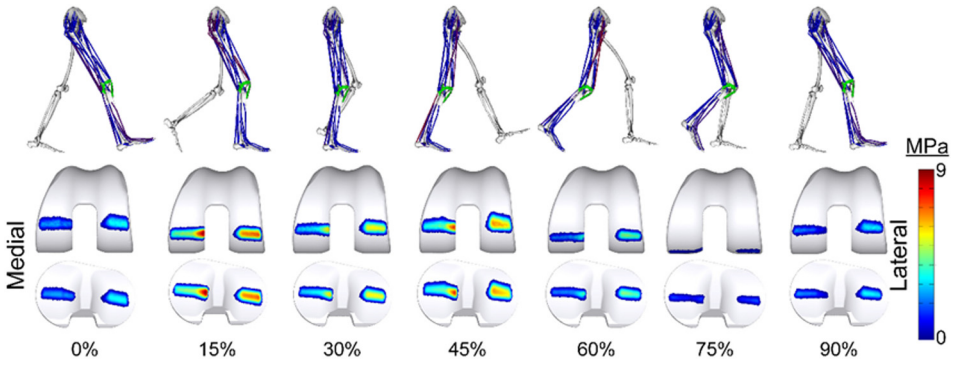

Fig. 3 Lower extremity posture, activated muscles (shown in red), and computed contact pressures on the femoral and tibial components throughout the smooth gait cycle (see online version for color)

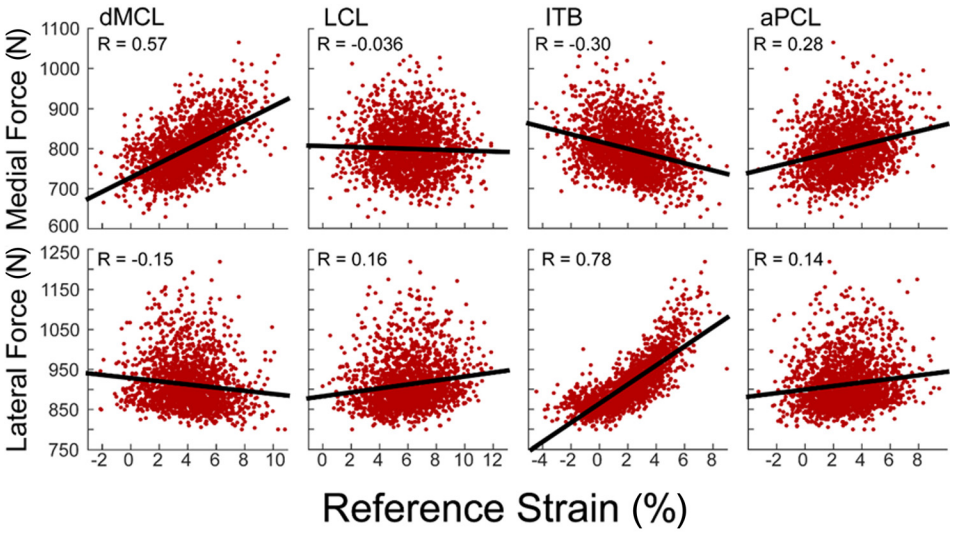

Fig. 4 Representative scatter plots showing the correlation between the second peak tibiofemoral contact forces and ligament reference strain. Each data point corresponds to 1 of the 2000 simulations run. The strength of the correlation between the predicted contact forces and the reference strain was evaluated using Pearson's correlation coefficients (*R*).

Table 2 Agreement between the measured and model (blind and unblind) predicted tibiofemoral joint contact forces during the smooth and bouncy gait trials

	Medial	Lateral	Total
Smooth gait			
ρ^2, squared Pearson's correlation coefficient			
Blinded	0.83	0.48	0.86
Unblinded	0.81	0.70	0.83
R^2, coefficient of determination			
Blinded	−0.47	0.19	0.68
Unblinded	0.71	0.56	0.79
Bias (BW)			
Blinded	0.44	−0.18	0.28
Unblinded	0.14	−0.06	0.10
Precision (BW)			
Blinded	0.27	0.24	0.30
Unblinded	0.19	0.21	0.32
rms error (BW)			
Blinded	0.52	0.29	0.40
Unblinded	0.23	0.22	0.33
Bouncy gait			
ρ^2, squared Pearson's correlation coefficient			
Blinded	0.80	0.42	0.82
Unblinded	0.70	0.61	0.72
R^2, coefficient of determination			
Blinded	−0.26	0.21	0.66
Unblinded	0.62	0.26	0.62
Bias (BW)			
Blinded	0.44	−0.14	0.30
Unblinded	0.12	0.06	0.18
Precision (BW)			
Blinded	0.25	0.26	0.34
Unblinded	0.25	0.28	0.44
rms error (BW)			
Blinded	0.50	0.29	0.45
Unblinded	0.28	0.29	0.48

The unblinded model included the subject-specific skeletal geometries and knee joint alignment as well as ligament attachments determined from the bone geometries. Unblinded total knee load predictions were substantially more consistent with measurements, with only a slight bias toward overprediction (smooth = 0.10 BW and bouncy = 0.18 BW). The temporal patterns of stance phase loading were well predicted on both compartments, while the late swing loading peak on the lateral compartment was predicted to occur slightly later than was measured (Fig. 5). Unblinded rms errors were reduced to 0.23 BW and 0.22 BW on the medial and lateral compartments, respectively, in the *smooth* gait trial. The corresponding coefficients of determination (R^2) were 0.71 and 0.56 for the medial and lateral compartments, respectively.

Coronal Alignment Effects. The coronal plane alignment of the TKR components had minimal effect on the net knee contact force over the entire gait cycle, but had a substantial effect on the medial–lateral distribution of the predicted contact forces during stance (Fig. 6). As expected, more varus alignments shifted the contact force distribution to the medial side of the joint, with the medial compartment supporting 42%, 54%, and 67% of the total predicted knee load at the first peak for the 4 deg valgus, nominal, and 4 deg varus component alignments, respectively. Similarly, the medial compartment accounted for 33%, 45%, and 58% of the total load at the second peak.

Probabilistic Ligament Simulations. The predicted ligament forces were relatively low with means of <50 N for each of the ligament bundles throughout the gait cycle (Fig. 7). The deep MCL, superficial MCL, and ITB remained engaged at relatively constant tensions throughout much of stance. The CAP and LCL forces exhibited a distinct peak of ~50 N when the knee was extended in late swing. The PFL and PCL exhibited peak loads just prior to toe-off and then remained engaged throughout swing.

There was substantial variability in predicted ligament forces due to uncertainty in ligament stiffness and reference strains (Fig. 7). The superficial MCL, deep MCL, PCL, and ITB forces were particularly sensitive in stance phase, with the 95% confidence intervals (CIs) extending from 0 to >100 N for each of these bundles. During swing, CAP and LCL forces were highly sensitive, with magnitudes that could vary from 0 to 100 N in terminal swing.

Ligament properties had substantial influence on the predicted medial and lateral contact forces (Fig. 8). The 95% CI of the predicted medial, lateral, and total contact force remained nearly

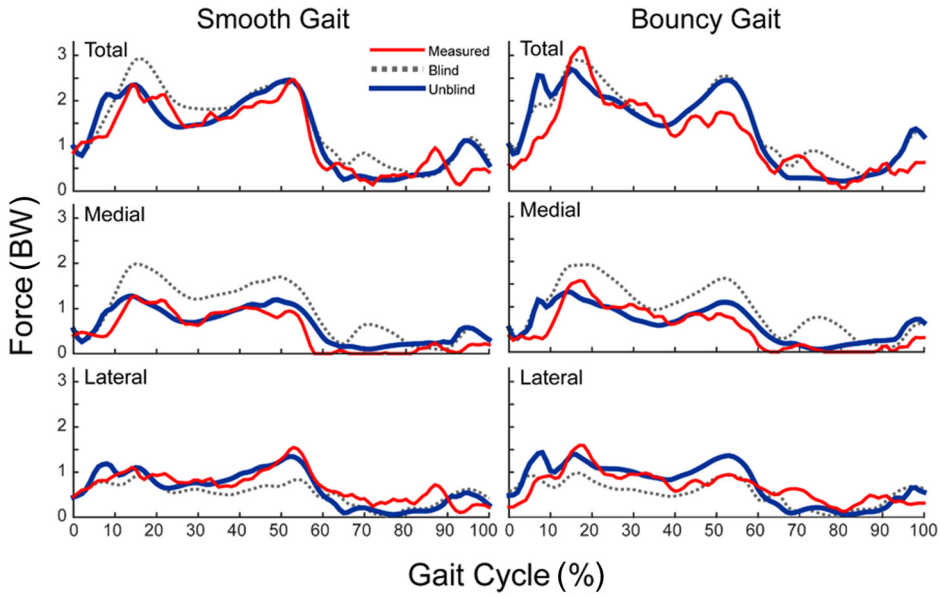

Fig. 5 Comparison of the blinded and unblinded model predicted tibial component contact forces (in tibia superior direction) to measured contact forces throughout the *smooth* and *bouncy* gait cycles. Error metrics are given in Table 2.

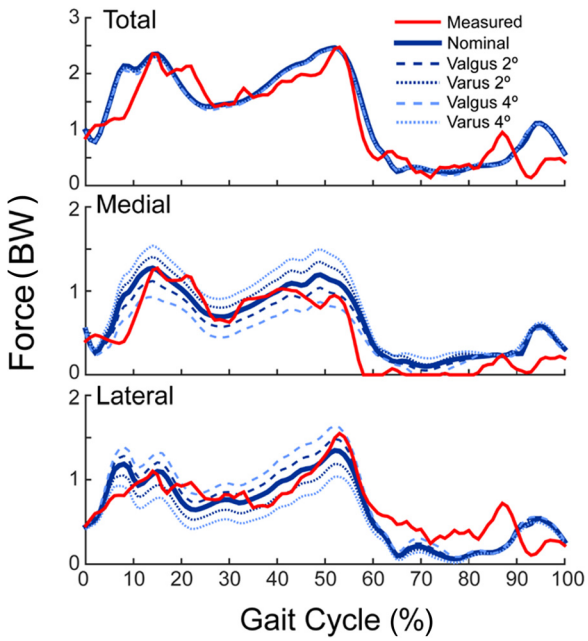

Fig. 6 Sensitivity of the joint contact forces to variations in coronal plane component alignment for *smooth* gait. Placing the components in a varus alignment relative to the nominal position shifted more of the total contact force to the medial compartment. The opposite relationship exists when placing the components in a valgus alignment, relative to nominal. Comparable results were found for *bouncy* gait.

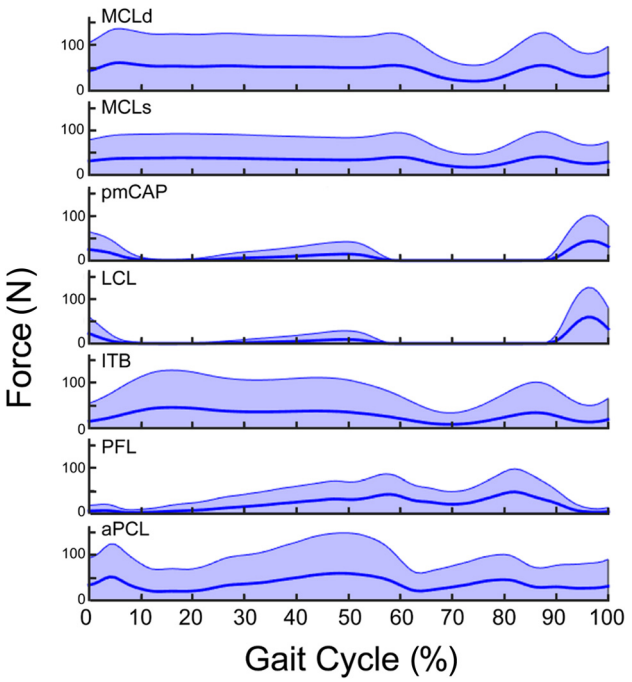

Fig. 7 Variability in ligament forces (shaded area represents the 95% confidence interval) throughout the *smooth* gait cycle due to uncertainty in ligament stiffness and reference strains. The dark center line is the mean of the Monte Carlo simulations, which is nearly identical to the force predicted by the nominal model.

constant (±0.2 BW) throughout the gait cycle with similar variability seen in the medial and lateral compartments.

For all the ligaments, the total contact force was positively correlated with ligament stiffness and reference strain (Fig. 9). The properties of the deep and superficial MCL had the primary influence on the predicted medial contact force at both first and second peak of tibiofemoral loading in stance. The reference strain of the aPCL was a secondary influence at both peaks and the reference strain of the pmCAP had influence at the second peak. The reference strain of the ITB showed a minor negative correlation throughout stance, acting to shift the load to the lateral compartment. The lateral contact force was primarily influenced by the properties of the ITB over the entire stance phase. At first peak, the ITB exhibited the highest correlation with load (stiffness: $R = 0.27$ and reference strain: $R = 0.81$) while the properties of both bundles of the MCL showed slight negative correlations. At the second peak, the ITB properties were again the primary

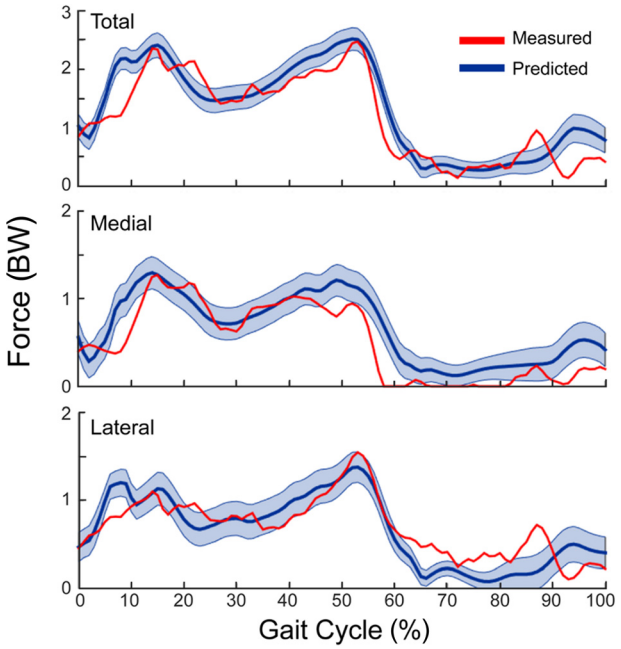

Fig. 8 Variability in predicted tibiofemoral joint contact forces (95% confience interval) throughout the *smooth* gait cycle due to uncertainty in the stiffness and reference strains assumed for ligaments

influence with the PFL, LCL and aPCL acting as secondary positive contributors.

Discussion

Our primary objective was to investigate the effect of TKR component alignment and ligament constitutive properties on tibiofemoral contact forces during gait. To accomplish this, we developed a subject-specific knee model, incorporated it into a lower extremity musculoskeletal model and then used numerical optimization to simultaneously predict muscle, ligament, and joint contact loads from motion analysis measures. We found that the incorporation of subject-specific component alignment was critical to achieve predictions of the medial–lateral contact force distributions that agreed with the measurements from an instrumented TKR. Our sensitivity analysis showed that the predicted ligament forces and medial–lateral contact force distributions were quite dependent on ligament stiffness and reference strain, with variations of ± 0.2 BW due to uncertainties in these parameters. Ligament properties are often manipulated in TKR procedures, such that our new simulation framework provides a viable approach for predicting the effects of TKR component designs and surgical techniques on postoperative knee function.

Musculoskeletal modeling and simulation techniques have notably advanced in recent years. The "Grand Challenge Competition to Predict in vivo Knee Loads" has contributed to this advance by providing rich subject-specific data sets of medical images, TKR geometries, motion analysis data, and joint contact load measurements, which allow researchers to benchmark various modeling techniques against each other. Prior approaches have included traditional optimization techniques to estimate muscle forces as inputs to finite-element models of the knee joint [20], EMG-driven simulations [21], and multibody dynamic simulations that include joint contact between articulating surfaces [22–24,]. The 2014 "Grand Challenge" winner introduced a unique optimization approach, termed force-dependent kinematics (FDK), that iteratively solved for the muscle forces and secondary tibiofemoral kinematics that balanced lower extremity dynamics [19]. However, that modeling approach pre-assumed an inextensible PT, resulting in an artificial kinematic constraint. We have extended the FDK approach by simultaneously solving the muscle forces, secondary tibiofemoral, and all patellofemoral kinematics that would induce the measured joint accelerations. Our joint contact load prediction errors (rms error = 0.33 BW in smooth gait) are comparable to that obtained using FDK (rms error = 0.26 BW), and slightly better than those that have been obtained using traditional optimization or forward dynamic simulations [18,23].

Our knee model and simulation technique includes several other notable features. The tibiofemoral and patellofemoral joints are each treated as 6DOF joints, with contact loads, muscle forces, and ligament tension contributing to joint stabilization. The model represented the ligaments as bundles of strands acting in parallel and included more passive structures of the knee than prior models. The ESO simulation routine provides for simultaneous estimates of muscle forces, ligament forces, joint contact pressures, and secondary kinematics at each time step, accounting for the inherent dynamic coupling between them. Of these, the joint contact pressures are particularly relevant in TKR given the links between

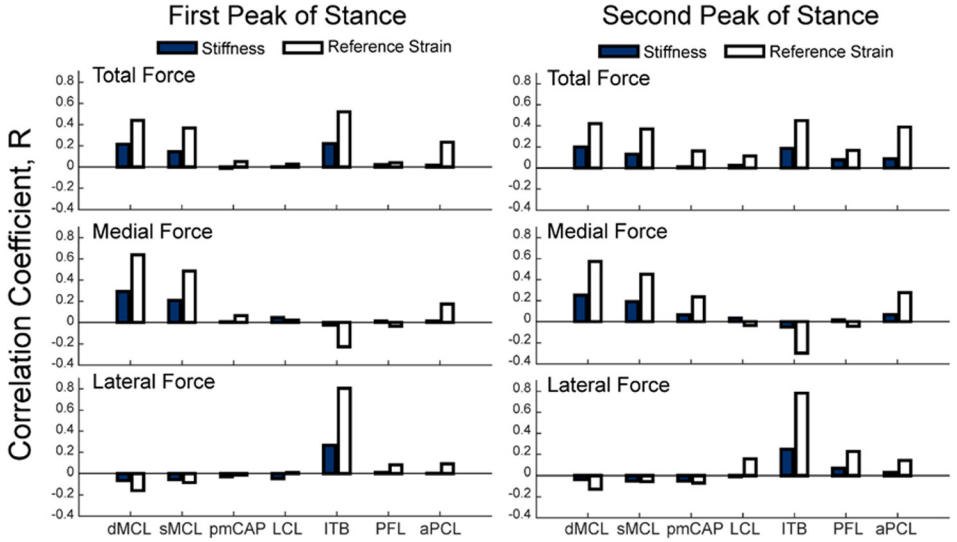

Fig. 9 Correlations of tibiofemoral contact forces with ligament stiffness (solid bars) and reference strain (open bars) at the first and second peaks of tibiofemoral loading during stance

the loading patterns and wear [63–67]. Finally, our simulation times were approximately 20 min per gait simulation on a traditional desktop computer (3.10 GHz Intel Xeon Processor, 16 GB RAM). As a result, by deploying simulations in parallel on a high throughput computing grid, 2000 probabilistic simulations can be performed in approximately 2 hrs. This capability allows the use of a Monte Carlo approach to quantitatively assess the influence of uncertain model parameters, such as ligament properties, on the knee joint contact.

In agreement with previous modeling studies [23,68,69], the coronal alignment of the femoral and tibial components affected the predicted knee contact loading patterns. While total contact force magnitudes were insensitive to alignment (Fig. 6), each 2 deg shift in valgus alignment resulted in equal (~0.15 BW) increases and decreases in the lateral and medial loads during stance, respectively. Accordingly, refining the TKR alignment in the model to better match the standing radiograph (Fig. 1) was the single most important factor that improved the agreement between our model predictions and measurements between the blinded and unblinded simulations (Fig. 5). In particular, our blinded model overpredicted the medial compartment contact forces resulting in an rms error of 0.52 BW in the smooth gait condition (Fig. 5). The coronal plane orientation of the components was adjusted in the unblinded model to closely match the valgus joint alignment seen in the standing radiographs (Fig. 1), resulting in substantially lower medial contact forces and rms errors (0.23 BW). This observation highlights the importance of considering subject-specific joint anatomy for characterizing mediolateral contact force distributions [70]. Furthermore, coronal plane alignment has been linked clinically to TKR component loosening and wear problems [7,71–76], such that our modeling framework could be further used to investigate the interaction of alignment, contact loads, and pressure patterns to understand how to better mitigate adverse TKR outcomes.

We systematically considered the influence of ligament properties on our predicted knee contact loading patterns. While prior models in the Grand Challenge Competition have included ligaments [18,19,22,23], our study is the first to consider the dependence of joint loading on uncertain ligament constitutive properties. The uncertainty analysis is important as there are currently no viable approaches for measuring ligament elasticity in vivo. As a result, ligament stiffness and reference strains must be estimated from cadaveric studies [23,34–37], which contributes to uncertainty in the model. Our results show total knee contact loads varied by ±0.2 BW (95% CIs) given our assumed uncertainty in ligament properties (Fig. 8), and that the total load increased monotonically with stiffness and reference strain for all the ligaments (Fig. 9). The latter result arises from the fact that our simulated tibiofemoral kinematics varied minimally with ligament properties, such that an increase in stiffness or reference strain (i.e., shorter slack length) enhanced the ligament tension and thus increased the contact load.

The influence of ligament stiffness and reference strain on the medial–lateral load distributions was highly variable between the ligaments and throughout the gait cycle (Fig. 9). MCL sensitivity was quite interesting with both the deep and superficial bundles exhibiting tensions that varied from 0 to ~100 N during stance (Fig. 7), depending on the properties assumed. Further, increased MCL tension induced an increase in medial compartment loading that exceeded a simultaneous decrease in lateral compartment loading. This is in agreement with a loaded cadaveric study which measured a 46% reduction in medial force and a 9% increase in lateral force at full extension following a major MCL release using an instrumented tibial insert [77]. Of the ligaments considered, lateral compartment loading was most sensitive to the ITB. Given the clinical significance of soft tissue balancing and known effects on long-term TKR function and longevity [66], our modeling framework may aid surgeons in positioning components and in planning soft tissue releases.

The results of this study highlight the clinical and modeling benefits of considering parameter uncertainty and sensitivity when performing musculoskeletal simulations. While previous editions of the Grand Challenge have focused largely on validation, sensitivity studies are also important to establish model credibility [25]. All the parameters of the musculoskeletal models have experimental errors associated with their values, and even in subject-specific models, many parameters must be estimated as they cannot be measured. Additionally, musculoskeletal models of the type used in this study can contain thousands of parameters, which makes them subject to redundancy, where multiple parameter combinations could result in agreement with the experimental measures. Accordingly, it is important to test the robustness of model predictions to a range of reasonable parameter values, particularly for parameters with large influence or variability [78]. In addition to complementing model validation, sensitivity studies are useful to reveal causal relationships between model parameters and simulated outcomes, making them highly relevant to surgical simulation.

To properly interpret the results of this study, several limitations in methodology must be noted. First, for computational reasons, joint contact pressures were computed using an elastic foundation model [54] rather than a finite-element model which could better characterize the component deformation state. The appropriateness of the elastic foundation model for estimating pressure has been previously established for TKR applications [79]. Additionally, the stiffness of polyethylene tibial insert was reduced by an order of magnitude to improve numerical stability of the optimization routine. The decreased stiffness resulted in slightly increased deformation and contact area, but had negligible effects on the secondary knee kinematics and net contact forces. Refined estimates of insert deformation and stress distributions could subsequently be obtained by using the net loads as boundary conditions on a finite-element model of the joint replacement.

We assumed muscle geometries based on a published generic musculoskeletal model [57] and assumed that muscle forces scaled linearly with activation. It would be reasonably straight forward to include subject-specific muscle geometry [80–82], if available, and to include more complex models of muscle–tendon dynamics [83,84] if the research application required more information on muscle behavior. We relied on numerical optimization to resolve muscle redundancy, a technique widely studied and used in biomechanics [85]. A traditional objective function based only on muscle activations [60] resulted in an overprediction of joint contact loads. Adding a penalty for high joint contact energy into the objective function (Eq. (2)) reduced knee contact forces, largely by redistributing loading among the plantarflexor muscles. Similarly, a prior EMG-informed model needed a constraint on the tibiofemoral contact forces in the model calibration phase [70] to prevent overprediction of contact loads. In this study, we imposed linear damping on the knee DOF to ensure the generation of smooth frame-to-frame kinematics. However, the damping force and moment magnitudes generated were relatively small, averaging less than 10 N and 1 N·m, respectively, over a gait cycle. Damping could alternatively be introduced into the model by including viscous effects present in ligaments and muscles.

The ligament attachment footprints in the model were determined relative to anatomical landmarks because magnetic resonance images were not available for the subject. However, the locations of ligament attachments in the knee joint relative to bony landmarks have been thoroughly documented in the literature [38–52]. The representation of each ligament bundle by many strands that span the attachment footprints may somewhat mitigate errors associated with single line of action ligament models. The Monte Carlo sampling distributions for the ligament properties were modeled as Gaussian, centered on nominal values derived from population-based studies [62]. This assumption was necessitated by the scarcity of experimental data and difficulty of measuring ligament properties in vivo. Finally, our sensitivity metrics from the Monte Carlo analysis are first-order correlation coefficients, which inherently do not account for nonlinearities or characterize interactions between the ligaments. The number of

simulations can easily be scaled up using high throughput computing platforms, allowing for more advanced sensitivity analyses [78,86] that consider parametric interactions.

In conclusion, we developed a subject-specific knee model and introduced a novel numerical optimization approach for predicting in vivo TKR mechanics during walking. Joint contact force predictions agreed very well with in vivo measurements obtained via an instrumented knee replacement. We also used the model to investigate the sensitivity of joint contact loading to component alignment and ligament properties. Thus, the proposed framework provides a viable objective approach for virtually designing TKR components, considering parametric uncertainty and predicting the effects of joint alignment and soft tissue balancing procedures on TKR function in movement.

Acknowledgment

We would like to thank B.J. Fregly, Ph.D., Darryl D'Lima, M.D., Ph.D., and the entire Grand Challenge team for organizing the competition and sharing the experimental data for this study. Additionally, we acknowledge Josh Roth for his contributions on the clinical interpretation of our research. This research was performed using the computing resources and assistance of the UW-Madison Center for High Throughput Computing.[2]

We gratefully acknowledge the support of NIH Grant Nos. AR065838, EB015410, and HD084213, and a NSF graduate research fellowship (MV) DGE-1256259.

References

[1] Fang, D. M., Ritter, M. A., and Davis, K. E., 2009, "Coronal Alignment in Total Knee Arthroplasty: Just How Important is It?" J. Arthroplasty, **24**(Suppl. 6), pp. 39–43.
[2] Insall, J., 1985, "Correction of Arthritic Deformities of the Knee," *Arthritis and Allied Conditions: A Textbook of Rheumatology*, 10th ed., Lea and Febiger, Philadelphia, PA, pp. 771–784.
[3] Sambatakakis, A., Wilton, T., and Newton, G., 1991, "Radiographic Sign of Persistent Soft-Tissue Imbalance After Knee Replacement," J. Bone Joint Surg., Br., **73**(5), pp. 751–756.
[4] Freeman, M., Todd, R., Bamert, P., and Day, W., 1978, "ICLH Arthroplasty of the Knee: 1968–1977," J. Bone Joint Surg., Br., **60**(3), pp. 339–344.
[5] Insall, J. N., Binazzi, R., Soudry, M., and Mestriner, L. A., 1985, "Total Knee Arthroplasty," Clin. Orthop. Relat. Res., **192**, pp. 13–22.
[6] Wasielewski, R. C., Galante, J. O., Leighty, R. M., Natarajan, R. N., and Rosenberg, A. G., 1994, "Wear Patterns on Retrieved Polyethylene Tibial Inserts and Their Relationship to Technical Considerations During Total Knee Arthroplasty," Clin. Orthop. Relat. Res., **299**, pp. 31–43.
[7] Windsor, R. E., Scuderi, G. R., Moran, M. C., and Insall, J. N., 1989, "Mechanisms of Failure of the Femoral and Tibial Components in Total Knee Arthroplasty," Clin. Orthop. Relat. Res., **248**, pp. 15–20.
[8] Lotke, P. A., and Ecker, M. L., 1977, "Influence of Positioning of Prosthesis in Total Knee Replacement," J. Bone Joint Surg., **59**(1), pp. 77–79.
[9] Karachalios, T., Sarangi, P., and Newman, J., 1994, "Severe Varus and Valgus Deformities Treated by Total Knee Arthroplasty," J. Bone Joint Surg., Br., **76**(6), pp. 938–942.
[10] Teeny, S. M., Krackow, K. A., Hungerford, D. S., and Jones, M., 1991, "Primary Total Knee Arthroplasty in Patients With Severe Varus Deformity. A Comparative Study," Clin. Orthop. Relat. Res., **273**, pp. 19–31.
[11] Dorr, L. D., and Boiardo, R. A., 1986, "Technical Considerations in Total Knee Arthroplasty," Clin. Orthop. Relat. Res., **205**, pp. 5–11.
[12] Matsuda, S., Miura, H., Nagamine, R., Urabe, K., Harimaya, K., Matsunobu, T., and Iwamoto, Y., 1999, "Changes in Knee Alignment After Total Knee Arthroplasty," J. Arthroplasty, **14**(5), pp. 566–570.
[13] Krackow, K. A., and Mihalko, W. M., 1998, "The Effect of Medial Release on Flexion and Extension Gaps in Cadaveric Knees: Implications for Soft-Tissue Balancing in Total Knee Arthroplasty," Am. J. Knee Surg., **12**(4), pp. 222–228.
[14] Whiteside, L. A., Saeki, K., and Mihalko, W. M., 2000, "Functional Medial Ligament Balancing in Total Knee Arthroplasty," Clin. Orthop. Relat. Res., **380**, pp. 45–57.
[15] Yagishita, K., Muneta, T., and Ikeda, H., 2003, "Step-by-Step Measurements of Soft Tissue Balancing During Total Knee Arthroplasty for Patients With Varus Knees," J. Arthroplasty, **18**(3), pp. 313–320.
[16] Scott, W. N., 2011, *Insall & Scott Surgery of the Knee*, Elsevier Health Sciences, Philadelphia, PA.
[17] Mihalko, W. M., Saleh, K. J., Krackow, K. A., and Whiteside, L. A., 2009, "Soft-Tissue Balancing During Total Knee Arthroplasty in the Varus Knee," J. Am. Acad. Orthop. Surg., **17**(12), pp. 766–774.
[18] Kinney, A. L., Besier, T. F., D'Lima, D. D., and Fregly, B. J., 2013, "Update on Grand Challenge Competition to Predict In Vivo Knee Loads," ASME J. Biomech. Eng., **135**(2), p. 021012.
[19] Marra, M. A., Vanheule, V., Fluit, R., Koopman, B. H., Rasmussen, J., Verdonschot, N., and Andersen, M. S., 2015, "A Subject-Specific Musculoskeletal Modeling Framework to Predict In Vivo Mechanics of Total Knee Arthroplasty," ASME J. Biomech. Eng., **137**(2), p. 020904.
[20] Kim, Y.-H., Park, W.-M., and Phuong, B. T. T., 2010, "Effect of Joint Center Location on In-Vivo Joint Contact Forces During Walking," ASME Paper No. SBC2010-19353.
[21] Manal, K., and Buchanan, T. S., 2013, "An Electromyogram-Driven Musculoskeletal Model of the Knee to Predict In Vivo Joint Contact Forces During Normal and Novel Gait Patterns," ASME J. Biomech. Eng., **135**(2), p. 021014.
[22] Guess, T. M., Stylianou, A. P., and Kia, M., 2014, "Concurrent Prediction of Muscle and Tibiofemoral Contact Forces During Treadmill Gait," ASME J. Biomech. Eng., **136**(2), p. 021032.
[23] Thelen, D. G., Choi, K. W., and Schmitz, A. M., 2014, "Co-Simulation of Neuromuscular Dynamics and Knee Mechanics During Human Walking," ASME J. Biomech. Eng., **136**(2), p. 021033.
[24] Hast, M. W., and Piazza, S. J., 2013, "Dual-Joint Modeling for Estimation of Total Knee Replacement Contact Forces During Locomotion," ASME J. Biomech. Eng., **135**(2), p. 021013.
[25] Anderson, A. E., Ellis, B. J., and Weiss, J. A., 2007, "Verification, Validation and Sensitivity Studies in Computational Biomechanics," Comput. Methods Biomech. Biomed. Eng., **10**(3), pp. 171–184.
[26] Chandrashekar, N., Mansouri, H., Slauterbeck, J., and Hashemi, J., 2006, "Sex-Based Differences in the Tensile Properties of the Human Anterior Cruciate Ligament," J. Biomech., **39**(16), pp. 2943–2950.
[27] Claes, L., Beyer, A., Krischke, W., and Schmid, R., 1987, "Biomechanical Properties of Collateral and Cruciate Ligaments. Biomechanics of Human Knee Ligaments," Proceedings of the European Society of Biomechanics, pp. 22.
[28] Noyes, F. R., and Grood, E. S., 1976, "The Strength of the Anterior Cruciate Ligament in Humans and Rhesus Monkeys," J. Bone Joint Surg., **58**(8), pp. 1074–1082.
[29] Prietto, M., Bain, J., Stonebrook, S., and Settlage, R., 1988, "Tensile Strength of the Human Posterior Cruciate Ligament (PCL)," Trans. Orthop. Res. Soc., **13**(195), pp. 736–745.
[30] Trent, P. S., Walker, P. S., and Wolf, B., 1976, "Ligament Length Patterns, Strength, and Rotational Axes of the Knee Joint," Clin. Orthop. Relat. Res., **117**, pp. 263–270.
[31] Woo, S. L.-Y., Hollis, J. M., Adams, D. J., Lyon, R. M., and Takai, S., 1991, "Tensile Properties of the Human Femur–Anterior Cruciate Ligament–Tibia Complex. The Effects of Specimen Age and Orientation," Am. J. Sports Med., **19**(3), pp. 217–225.
[32] Fregly, B. J., Besier, T. F., Lloyd, D. G., Delp, S. L., Banks, S. A., Pandy, M. G., and D'Lima, D. D., 2012, "Grand Challenge Competition to Predict In Vivo Knee Loads," J. Orthop. Res., **30**(4), pp. 503–513.
[33] Meyer, A. J., D'Lima, D. D., Banks, S. A., Coburn, J., Harman, M., Mikashima, Y., and Fregly, B. J., 2011, "Evaluation of Regression Equations for Medial and Lateral Contact Force From Instrumented Knee Implant Data," ASME Paper No. SBC2011-53938.
[34] Smith, C. R., Lenhart, R. L., Kaiser, J., Vignos, M. F., and Thelen, D. G., "Influence of Ligament Properties on Tibiofemoral Mechanics in Walking," J. Knee Surg. (in press).
[35] Blankevoort, L., and Huiskes, R., 1991, "Ligament–Bone Interaction in a Three-Dimensional Model of the Knee," ASME J. Biomech. Eng., **113**(3), pp. 263–269.
[36] Shelburne, K. B., Pandy, M. G., Anderson, F. C., and Torry, M. R., 2004, "Pattern of Anterior Cruciate Ligament Force in Normal Walking," J. Biomech., **37**(6), pp. 797–805.
[37] Shin, C. S., Chaudhari, A. M., and Andriacchi, T. P., 2007, "The Influence of Deceleration Forces on ACL Strain During Single-Leg Landing: A Simulation Study," J. Biomech., **40**(5), pp. 1145–1152.
[38] Amis, A., Firer, P., Mountney, J., Senavongse, W., and Thomas, N., 2003, "Anatomy and Biomechanics of the Medial Patellofemoral Ligament," Knee, **10**(3), pp. 215–220.
[39] Amis, A., Gupte, C., Bull, A., and Edwards, A., 2006, "Anatomy of the Posterior Cruciate Ligament and the Meniscofemoral Ligaments," Knee Surg. Sports Traumatol. Arthroscopy, **14**(3), pp. 257–263.
[40] Basso, O., Johnson, D., and Amis, A., 2001, "The Anatomy of the Patellar Tendon," Knee Surg. Sports Traumatol. Arthroscopy, **9**(1), pp. 2–5.
[41] Edwards, A., Bull, A. M., and Amis, A. A., 2007, "The Attachments of the Fiber Bundles of the Posterior Cruciate Ligament: An Anatomic Study," Arthroscopy, **23**(3), pp. 284–290.
[42] Ferretti, M., Ekdahl, M., Shen, W., and Fu, F. H., 2007, "Osseous Landmarks of the Femoral Attachment of the Anterior Cruciate Ligament: An Anatomic Study," Arthroscopy, **23**(11), pp. 1218–1225.
[43] Giron, F., Cuomo, P., Aglietti, P., Bull, A. M., and Amis, A. A., 2006, "Femoral Attachment of the Anterior Cruciate Ligament," Knee Surg. Sports Traumatol. Arthroscopy, **14**(3), pp. 250–256.
[44] Kopf, S., Musahl, V., Tashman, S., Szczodry, M., Shen, W., and Fu, F. H., 2009, "A Systematic Review of the Femoral Origin and Tibial Insertion Morphology of the ACL," Knee Surg. Sports Traumatol. Arthroscopy, **17**(3), pp. 213–219.

[2] www.chtc.cs.wisc.edu

[45] LaPrade, R. F., Ly, T. V., Wentorf, F. A., and Engebretsen, L., 2003, "The Posterolateral Attachments of the Knee a Qualitative and Quantitative Morphologic Analysis of the Fibular Collateral Ligament, Popliteus Tendon, Popliteofibular Ligament, and Lateral Gastrocnemius Tendon," Am. J. Sports Med., **31**(6), pp. 854–860.
[46] Liu, F., Yue, B., Gadikota, H. R., Kozanek, M., Liu, W., Gill, T. J., Rubash, H. E., and Li, G., 2010, "Morphology of the Medial Collateral Ligament of the Knee," J. Orthop. Surg. Res., **5**(1), pp. 1–8.
[47] Meister, B. R., Michael, S. P., Moyer, R. A., Kelly, J. D., and Schneck, C. D., 2000, "Anatomy and Kinematics of the Lateral Collateral Ligament of the Knee," Am. J. Sports Med., **28**(6), pp. 869–878.
[48] Nomura, E., Inoue, M., and Osada, N., 2005, "Anatomical Analysis of the Medial Patellofemoral Ligament of the Knee, Especially the Femoral Attachment," Knee Surg. Sports Traumatol. Arthroscopy, **13**(7), pp. 510–515.
[49] Rachmat, H., Janssen, D., Zevenbergen, W., Verkerke, G., Diercks, R., and Verdonschot, N., 2014, "Generating Finite Element Models of the Knee: How Accurately Can We Determine Ligament Attachment Sites From MRI Scans?" Med. Eng. Phys., **36**(6), pp. 701–707.
[50] Robinson, J., Sanchez-Ballester, J., Bull, A., de, WM, Thomas, R., and Amis, A., 2004, "The Posteromedial Corner Revisited. An Anatomical Description of the Passive Restraining Structures of the Medial Aspect of the Human Knee," J. Bone Joint Surg., Br., **86**(5), pp. 674–681.
[51] Sugita, T., and Amis, A. A., 2001, "Anatomic and Biomechanical Study of the Lateral Collateral and Popliteofibular Ligaments," Am. J. Sports Med., **29**(4), pp. 466–472.
[52] Wijdicks, C. A., Griffith, C. J., LaPrade, R. F., Johansen, S., Sunderland, A., Arendt, E. A., and Engebretsen, L., 2009, "Radiographic Identification of the Primary Medial Knee Structures," J. Bone Joint Surg., **91**(3), pp. 521–529.
[53] Vignos, M. F., Smith, C. R., and Thelen, D. G., 2015, "Automated Method for Discretizing Ligaments in Musculoskeletal Simulation Models," 13th International Symposium on Computer Methods in Biomechanics and Biomedical Engineering (CMBBE), Montreal, QC, Canada, Sept. 1–5.
[54] Bei, Y., and Fregly, B. J., 2004, "Multibody Dynamic Simulation of Knee Contact Mechanics," Med. Eng. Phys., **26**(9), pp. 777–789.
[55] Kurtz, S., Jewett, C., Bergström, J., Foulds, J., and Edidin, A., 2002, "Miniature Specimen Shear Punch Test for UHMWPE Used in Total Joint Replacements," Biomaterials, **23**(9), pp. 1907–1919.
[56] Bartel, D., Rawlinson, J., Burstein, A., Ranawat, C., and Flynn, W., Jr., 1995, "Stresses in Polyethylene Components of Contemporary Total Knee Replacements," Clin. Orthop. Relat. Res., **317**, pp. 76–82.
[57] Arnold, E. M., Ward, S. R., Lieber, R. L., and Delp, S. L., 2010, "A Model of the Lower Limb for Analysis of Human Movement," Ann. Biomed. Eng., **38**(2), pp. 269–279.
[58] Jeffery, R. S., Morris, R. W., and Denham, R. A., 1991, "Coronal Alignment After Total Knee Replacement," J. Bone Joint Surg., Br., **73**(5), pp. 709–714.
[59] Delp, S. L., and Loan, J. P., 2000, "A Computational Framework for Simulating and Analyzing Human and Animal Movement," Comput. Sci. Eng., **2**(5), pp. 46–55.
[60] Happee, R., 1994, "Inverse Dynamic Optimization Including Muscular Dynamics: A New Simulation Method Applied to Goal Directed Movements," J. Biomech., **27**(7), pp. 953–960.
[61] Lenhart, R. L., Kaiser, J., Smith, C. R., and Thelen, D. G., 2015, "Prediction and Validation of Load-Dependent Behavior of the Tibiofemoral and Patellofemoral Joints During Movement," Ann. Biomed. Eng., **43**(11), pp. 2675–2685.
[62] Baldwin, M. A., Laz, P. J., Stowe, J. Q., and Rullkoetter, P. J., 2009, "Efficient Probabilistic Representation of Tibiofemoral Soft Tissue Constraint," Comput. Methods Biomech. Biomed. Eng., **12**(6), pp. 651–659.
[63] Reinders, J., Sonntag, R., Vot, L., Gibney, C., Nowack, M., and Kretzer, J. P., 2015, "Wear Testing of Moderate Activities of Daily Living Using In Vivo Measured Knee Joint Loading," PloS One, **10**(3), p. e0123155.
[64] Wimmer, M., Knowlton, C., Pourzal, R., McEwen, P., and Andriacchi, T., 2013, "Clinical TKA Wear Rates and Their Association With Gait Parameters," Bone Joint J. Orthop. Proc. Suppl., **95**(Suppl. 34), pp. 587.
[65] Abdel-Jaber, S., Belvedere, C., Leardini, A., and Affatato, S., 2015, "Wear Simulation of Total Knee Prostheses Using Load and Kinematics Waveforms From Stair Climbing," J. Biomech., **48**(14), pp. 3830–3836.
[66] Babazadeh, S., Stoney, J. D., Lim, K., and Choong, P. F., 2009, "The Relevance of Ligament Balancing in Total Knee Arthroplasty: How Important is It? A Systematic Review of the Literature," Orthop. Rev., **1**(2), p. e26.
[67] Fregly, B. J., Sawyer, W. G., Harman, M. K., and Banks, S. A., 2005, "Computational Wear Prediction of a Total Knee Replacement From In Vivo Kinematics," J. Biomech., **38**(2), pp. 305–314.
[68] Lerner, Z. F., DeMers, M. S., Delp, S. L., and Browning, R. C., 2015, "How Tibiofemoral Alignment and Contact Locations Affect Predictions of Medial and Lateral Tibiofemoral Contact Forces," J. Biomech., **48**(4), pp. 644–650.
[69] Chen, Z., Wang, L., Liu, Y., He, J., Lian, Q., Li, D., and Jin, Z., 2015, "Effect of Component Mal-Rotation on Knee Loading in Total Knee Arthroplasty Using Multi-Body Dynamics Modeling Under a Simulated Walking Gait," J. Orthop. Res., **33**(9), pp. 1287–1296.
[70] Gerus, P., Sartori, M., Besier, T. F., Fregly, B. J., Delp, S. L., Banks, S. A., Pandy, M. G., D'Lima, D. D., and Lloyd, D. G., 2013, "Subject-Specific Knee Joint Geometry Improves Predictions of Medial Tibiofemoral Contact Forces," J. Biomech., **46**(16), pp. 2778–2786.
[71] Srivastava, A., Lee, G. Y., Steklov, N., Colwell, C. W., Jr., Ezzet, K. A., and D'Lima, D. D., 2012, "Effect of Tibial Component Varus on Wear in Total Knee Arthroplasty," Knee, **19**(5), pp. 560–563.
[72] Ritter, M. A., Faris, P. M., Keating, E. M., and Meding, J. B., 1994, "Postoperative Alignment of Total Knee Replacement Its Effect on Survival," Clin. Orthop. Relat. Res., **299**, pp. 153–156.
[73] Feng, E. L., Stulberg, S. D., and Wixson, R. L., 1994, "Progressive Subluxation and Polyethylene Wear in Total Knee Replacements With Flat Articular Surfaces," Clin. Orthop. Relat. Res., **299**, pp. 60–71.
[74] D'Lima, D. D., Hermida, J. C., Chen, P. C., and Colwell, C. W., Jr., 2001, "Polyethylene Wear and Variations in Knee Kinematics," Clin. Orthop. Relat. Res., **392**, pp. 124–130.
[75] Hernigou, P., and Deschamps, G., 2004, "Alignment Influences Wear in the Knee After Medial Unicompartmental Arthroplasty," Clin. Orthop. Relat. Res., **423**, pp. 161–165.
[76] Werner, F. W., Ayers, D. C., Maletsky, L. P., and Rullkoetter, P. J., 2005, "The Effect of Valgus/Varus Malalignment on Load Distribution in Total Knee Replacements," J. Biomech., **38**(2), pp. 349–355.
[77] Crottet, D., Kowal, J., Sarfert, S. A., Maeder, T., Bleuler, H., Nolte, L.-P., and Dürselen, L., 2007, "Ligament Balancing in TKA: Evaluation of a Force-Sensing Device and the Influence of Patellar Eversion and Ligament Release," J. Biomech., **40**(8), pp. 1709–1715.
[78] Hicks, J. L., Uchida, T. K., Seth, A., Rajagopal, A., and Delp, S. L., 2015, "Is My Model Good Enough? Best Practices for Verification and Validation of Musculoskeletal Models and Simulations of Movement," ASME J. Biomech. Eng., **137**(2), p. 020905.
[79] Halloran, J. P., Easley, S. K., Petrella, A. J., and Rullkoetter, P. J., 2005, "Comparison of Deformable and Elastic Foundation Finite Element Simulations for Predicting Knee Replacement Mechanics," ASME J. Biomech. Eng., **127**(5), pp. 813–818.
[80] Scheys, L., Loeckx, D., Spaepen, A., Suetens, P., and Jonkers, I., 2009, "Atlas-Based Non-Rigid Image Registration to Automatically Define Line-of-Action Muscle Models: A Validation Study," J. Biomech., **42**(5), pp. 565–572.
[81] Blemker, S. S., Asakawa, D. S., Gold, G. E., and Delp, S. L., 2007, "Image-Based Musculoskeletal Modeling: Applications, Advances, and Future Opportunities," J. Magn. Reson. Imaging, **25**(2), pp. 441–451.
[82] Valente, G., Pitto, L., Testi, D., Seth, A., Delp, S. L., Stagni, R., Viceconti, M., and Taddei, F., 2014, "Are Subject-Specific Musculoskeletal Models Robust to the Uncertainties in Parameter Identification?" PLoS One, **9**(11), p. e112625.
[83] Thelen, D. G., 2003, "Adjustment of Muscle Mechanics Model Parameters to Simulate Dynamic Contractions in Older Adults," ASME J. Biomech. Eng., **125**(1), pp. 70–77.
[84] Millard, M., Uchida, T., Seth, A., and Delp, S. L., 2013, "Flexing Computational Muscle: Modeling and Simulation of Musculotendon Dynamics," ASME J. Biomech. Eng., **135**(2), p. 021005.
[85] Erdemir, A., McLean, S., Herzog, W., and van den Bogert, A. J., 2007, "Model-Based Estimation of Muscle Forces Exerted During Movements," Clin. Biomech., **22**(2), pp. 131–154.
[86] Laz, P., and Browne, M., 2010, "A Review of Probabilistic Analysis in Orthopaedic Biomechanics," Proc. Inst. Mech. Eng., Part H, **224**(8), pp. 927–943.